ACS APPLIED MATERIALS & INTERFACES

Research Article

www.acsami.org

Highly Efficient and Large-Scale Fabrication of Superhydrophobic Alumina Surface with Strong Stability Based on Self-Congregated Alumina Nanowires

Shan Peng, Dong Tian, Xiaojun Yang, and Wenli Deng*

College of Materials Science and Engineering, South China University of Technology, Guangzhou 510640, P. R. China

Supporting Information

ABSTRACT: In this study, a large-area superhydrophobic alumina surface with a series of superior properties was fabricated via an economical, simple, and highly effective one-step anodization process, and subsequently modified with low-surface-energy film. The effects of the anodization parameters including electrochemical anodization time, current density, and electrolyte temperature on surface morphology and surface wettability were investigated in detail. The hierarchical alumina pyramids-on-pores (HAPOP) rough structure which was produced quickly through the one-step anodization process together with a low-surface-energy film deposition [1*H*,1*H*,2*H*,2*H*-perfluorodecyltriethoxysilane (PDES) and stearic acid (STA)] confer excellent superhydrophobicity and an extremely low sliding angle. Both the PDES-modified superhydrophobic (PDES-MS) and the STA-modified superhydrophobic (STA-MS) surfaces present fascinating nonwetting and extremely slippery behaviors. The chemical stability and mechanical durability of the PDES-MS and STA-MS surfaces were evaluated and discussed. Compared with the STA-MS surface, the as-prepared PDES-MS surface possesses an amazing chemical stability which not only can repel cool liquids (water, HCl/NaOH solutions, around 25 °C), but also can show excellent resistance to a series of hot liquids (water, HCl/NaOH solutions, 30−100 °C) and hot beverages (coffee, milk, tea, 80 °C). Moreover, the PDES-MS surface also presents excellent stability toward immersion in various organic solvents, high temperature, and long time period. In particular, the PDES-MS surface achieves good mechanical durability which can withstand ultrasonication treatment, finger-touch, multiple fold, peeling by adhesive tape, and even abrasion test treatments without losing superhydrophobicity. The corrosion resistance and durability of the diverse-modified superhydrophobic surfaces were also examined. These fascinating performances makes the present method suitable for large-scale industrial fabrication of chemically stable and mechanically robust superhydrophobic surfaces.

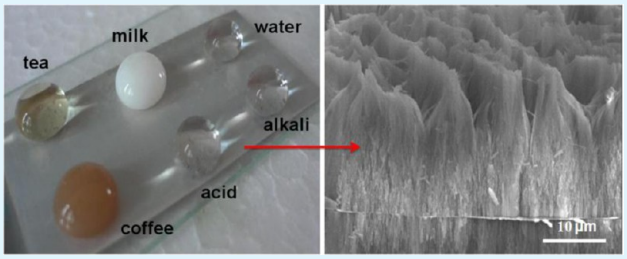

KEYWORDS: *hierarchical structures, aluminum, superhydrophobicity, electrochemical anodization, stability, mechanical durability, surface free energy*

1. INTRODUCTION

Many plants and animals such as lotus leaves (*Nelumbo nucifera*), *Gerris remigis*, and gecko feet naturally inherit superhydrophobic surfaces.[1−3] In general, to obtain superhydrophobic surfaces that show water contact angle (WCA) greater than 150° and sliding angle (SA) less than 10°, significant surface roughness or low surface energy should be required.[4,5] Inspired from the excellent nonwetting and self-cleaning properties of lotus leaves, researchers have developed a large number of techniques to fabricate superhydrophobic surfaces to achieve high WCAs and low SAs, such as layer-by-layer deposition,[6] hydrothermal synthesis,[7] chemical etching,[8,9] electrospinning,[10,11] colloidal coating,[12,13] and anodic oxidation.[14−16] However, although many artificial superhydrophobic surfaces have been reported in the past years, a lot of practical problems exist when they have been applied in daily life and industrial areas. On one hand, from the perspective of chemical stability, many superhydrophobic surfaces would immediately lose the superhydrophobicity when they are exposed to complex and rigorous conditions such as strong acid/alkali solutions, high temperature, hot liquids, oil contamination, or solvent contamination, showing bad chemical stability. With hot water as an example, most of the previously reported superhydrophobic surfaces could only repel cold water under room temperature (around 25 °C), but show remarkably decreased repellency to hot water (50 °C or higher). As we know, it is not difficult to fabricate superhydrophobic surfaces that repel cool water because of its higher surface tension of 72.8 mN m^{-1}. However, since the surface tension of hot water decreases with increasing temperature, many superhydrophobic surfaces including natural lotus leaves cannot resist hot water,[17] to say nothing of hot strong acid/alkali solutions or hot

Received: December 16, 2013
Accepted: March 4, 2014
Published: March 4, 2014

   dx.doi.org/10.1021/am4057858 | *ACS Appl. Mater. Interfaces* 2014, 6, 4831−4841

beverages (coffee, tea, milk, etc.), which confines their practical applications to a great extent. To the best of our knowledge, there are few previous papers reporting the repellency of superhydrophobic surfaces to hot water and even fewer to hot corrosive solutions or beverages.[17] On the other hand, the inability to find practical applications for most of the superhydrophobic products is mainly ascribed to their bad mechanical properties and abrasion resistance. For example, when the abrasion test is applied with pressure and shear force on the superhydrophobic surface, the microprotuberances are easily broken and the surfaces quickly become flat, leading to damage of superhydrophobic effects. Moreover, some superhydrophobic membranes are easily peeled off and removed, presenting a weak attachment with the substrate.[18,19] For the above-mentioned reasons, it is of great significance to prepare superhydrophobic surfaces with excellent chemical stability and mechanical durability when considering practical applications of superhydrophobic surfaces.

Aluminum and its alloys are important industrial materials due to their low weight, superior electronic and thermal conductivity, and excellent corrosion resistance. In recent years, although a variety of synthetic techniques have been developed to fabricate superhydrophobic surfaces on Al and its alloys,[20−27] methods such as chemical vapor deposition, chemical etching, or hydrothermal reaction could only be used in the laboratory in small scale. In comparison, the anodization technique is a very promising method to produce self-organized nanostructures over large surface area. Moreover, it is also one of the most economical, simple, and efficient methods to construct superhydrophobic surfaces on metal substrates.[28−30] Recently, although great progress has been made to fabricate mechanically robust superhydrophobic surfaces,[21,31−35] only limited success has been achieved in fabricating chemically stable and mechanically robust superhydrophobic Al surfaces.[16,21,31] For example, Bae et al. fabricated a robust superhydrophobic Al alloy by using a wire electrical discharge machining method.[21] Barthwal et al. reported a mechanically robust superamphiphobic aluminum surface by a combination of simple chemical etching and anodization approach.[31] However, these methods have potential weaknesses such as requiring complex equipment or time-consuming multiple steps to obtain superhydrophobic surface, which are not simple and convenient enough. Moreover, the comprehensive evaluation and study of the chemical resistance (such as resistance to hot liquids) and mechanical durability of the superhydrophobic Al surfaces are scarcely involved in these reports. In addition, little information is currently available about the wettability and performance comparisons of the solid surfaces modified by materials with diverse surface free energy.[36,37]

In this paper, a simple and highly efficient anodized method was used to prepare chemically stable and mechanically durable superhydrophobic alumina surface on an aluminum substrate. In order to confirm the best preparation parameters to fabricate the rough HAPOP morphology, the effects of the anodized parameters including current density, electrochemical anodization time, and electrolyte temperature on surface topography and surface wettability were studied systematically. These parameters determine the surface architectures that influence the hydrophobicity. It is found that the hierarchical alumina pyramids-on-pores structure, which can be formed quickly within 10 min at a current density of 0.16 A/cm^2, is indispensible for obtaining a superhydrophobic surface. We modified the as-prepared surfaces by using PDES and STA materials. The chemical stability and mechanical durability of the superhydrophobic surfaces are evaluated and studied by a variety of methods. The obtained results indicate that the PDES-MS surface presents an outstanding stability against numerous harsh conditions such as hot water (30−100 °C), hot corrosive liquids (HCl/NaOH solutions, 30−100 °C), hot beverages (coffee, milk, tea, 80 °C), immersion in various solvents, high temperature, and long time period. Furthermore, it also exhibits excellent mechanical properties which could resist ultrasonication treatment, finger touching, multiple folding, peeling by adhesive tape, and even abrasion test treatments. In the case of the STA-MS surface, WCA and SA of 153° and 0°, respectively, can be obtained. It presents superoleophilicity with a hexadecane CA of 0°. The chemical stability and mechanical durability of the STA-MS surface were also examined, which was demonstrated to be much worse than PDES-MS.

2. EXPERIMENTAL SECTION

2.1. Materials. All chemicals were analytical grade and used as received. The available aluminum plates (composition: Al of wt 98%, Si of 0.3%, O of 1.7%), STA (stearic acid), and oxalic acid were all obtained from Guangzhou QianHui materials Co., PR China; PDES [1*H*,1*H*,2*H*,2*H*-perfluorodecyltriethoxysilane] was obtained from Alfa Aesar Co., PR China.

2.2. Specimen Preparation. Prior to electrochemical anodization, the Al plates (50 mm × 15 mm) were sequentially cleaned with acetone, ethanol, and deionized water by ultrasonication. Then, one-step electrochemical anodization was applied for preparation after the Al samples were dried. The aluminum plate and platinum were used as anode and cathode, respectively. The cleaned Al plates were anodized in 0.3 M oxalic acid electrolyte at a 0.16 A/cm^2 current density at room temperature for 10 min and the targeted hierarchical alumina surfaces could be obtained (the anodization voltage was 112 V first; however, it decreased to 81 V after the 10 min reaction process). The as-prepared samples were next ultrasonically rinsed with deionized water and subsequently dried. The obtained specimens were immersed in 1.0 wt % ethanol solution of PDES for 30 min and 5 mM ethanol solution of STA for 4 h. Finally, the obtained samples were heated at 80 °C for 30 min.

2.3. Specimen Characterization. The surface structures of the as-prepared samples were observed under a field emission scanning electron microscopy (FESEM, NOVA NANOSEM 430). The surface compositions were investigated using energy dispersive spectroscopy (EDS) (Oxford X-Max 20, England) and X-ray photoelectron spectroscopy (XPS) (Kratos AXis Ultra X-ray photoelectron spectroscopy). The water contact angles (WCAs) and sliding angles (SAs) were obtained on OCA35 (DataPhysics, Germany) equipped with a video camera and a tilting stage. SAs were measured by slowly tilting the sample stage until the water droplet started moving. The static WCA and SA values were the averages of five measurements obtained at diverse positions by using 3−5 μL water drops. The optical pictures were obtained by a digital camera (Canon).The electrochemical measurements were conducted in 3.5 wt % aqueous solutions of NaCl at room temperature using electrochemical workstation (IM6ex, Zahner, Germany). The electrochemical corrosion tests were carried out using a three-electrode configuration with platinum as the counter electrode, saturated calomel as the reference electrode, and the samples with an exposed area of 1 cm^2 as the working electrode.

3. RESULTS AND DISCUSSION

3.1. Effects of Various Experimental Parameters on Surface Morphology and Surface Wettability. To better understand the formation procedure of the superhydrophobic alumina surface, the effects of anodized time, anodized current density, and electrolyte temperature on surface morphology are

investigated in detail. Figure 1 presents the FESEM images of an aluminum surface electrochemically anodized for different

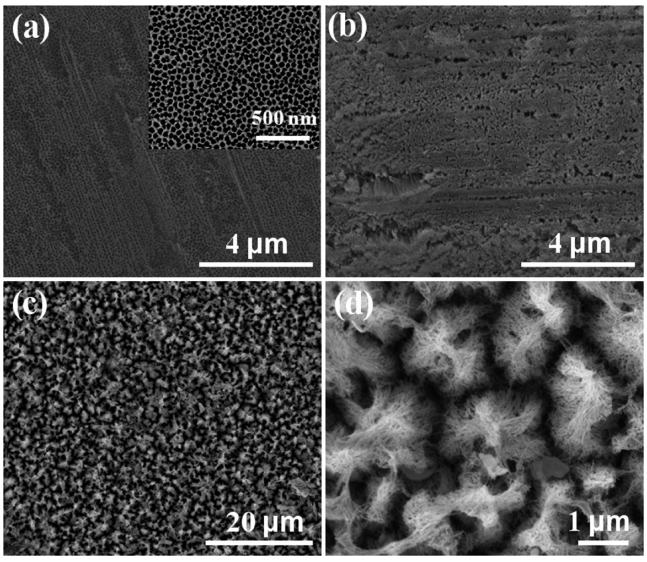

Figure 1. FESEM images of the anodized alumina membranes obtained at 0.16 A/cm^2 processing current density at room temperature with diverse processing time ranging from 3 to 10 min: (a) 3 min, (b) 5 min, (c) 10 min, (d) a high-magnification picture of (c). The inset of (a) is its high-magnification image.

times ranging from 3 to 10 min in 0.3 M oxalic acid solution under room temperature at a 0.16 A/cm^2 current density, which exhibits a dynamic evolution process of surface topography from nanopores, nanowire arrays, and then to congregated nanowire pyramids. Under the relatively higher current density, the whole process was finished in a very short time, within 10 min. During the first 3 min, the common nanoscale porous anodic alumina oxide (AAO) structure with the diameter of about 100 nm formed rapidly (Figure 1a). However, owing to the higher current density and the unpolished raw aluminum plate, the nanoporous surface was very uneven and irregular and some obviously broken nanoporous could be observed clearly from the surface. With the increasing anodization time to 5 min, it was found that large-area dense nanowire arrays formed in this stage (Figure 1b). The nanopores in the upper layer totally transformed into nanowires. It was obvious that the nanowire arrays were short and closely aligned with each other. However, when the anodization time was prolonged to 10 min, a kind of protrusion and ravine structure was formed on the surface (Figure 1c). When viewed from the higher-magnification SEM image, we found that large amounts of nanowires with high aspect ratio intertwined and congregated with each other, forming the micropyramid morphology with diameter of about 3 μm (Figure 1d).

The typical side-view SEM images corresponding to the structures shown in Figure 1 were demonstrated in Figure 2. The height of the AAO nanopore structure was more than 15 μm (Figure 2a). After anodization for 5 min, the top region of nanopores was etched into nanowires with length less than 5 μm (Figure 2b). When the anodized time was 10 min, large-area high-aspect-ratio nanowires with height of more than 15 μm formed (Figure 2c). It also demonstrated that the nanopore structure almost totally turned into nanowires with the increasing anodized time, and we could clearly observe that the nanowires tended to aggregate into bunches (Figure 2c), thus leaving the ravine morphology among the pyramidal structure.

The microravine and micropyramid structures form on the surface through a self-assembly process of the nanowires, while the bottom nanopore morphology is retained, constructing a kind of hierarchical topography. The formation mechanisms of anodized alumina nanowire morphology have been proposed in previous studies.[38,39] In this work, we ascribe the fast formation of the hierarchical alumina pyramids-on-pores structure to the following reasons. First, the electrical potential is a decisive factor in effecting the formation speed and the diameter of the alumina nanopores.[40] The nanopore structure forms more quickly under a higher current density. However, with the increasing anodization time, the higher electrical potential energy could break down the nanoporous structure instantaneously. Once the original nanopore morphology was interrupted and expanded, the nanowalls would get etched and thinned more easily. Owing to the higher acid concentration, the structure on the top layer broke and thinned first, finally resulting in producing nanowires in a very short time. The second significant factor is the large quantity of heat induced by the strong electrical potential energy. The drastic anodized reaction phenomenon can be observed clearly during the experimental process, thus arousing the increasing heat, which cannot diffuse immediately. This phenomenon would make the volume-expansion more serious and finally cause the severe interruption and destruction of the pristine nanopore structure, which would further accelerate the dissolution of nanowalls. With the increasing reaction time, the nanowires become longer and longer. Due to the gravity and stirring effects, these longer nanowires are inclined to collapse and align with each other from the diverse directions to form the micropyramid structure, thus simultaneously producing the ravine topography among the pyramids.

The FESEM images of the anodized alumina surfaces fabricated by regulating the current densities were shown in Figure 3. The other parameters were conducted at 0.3 M oxalic

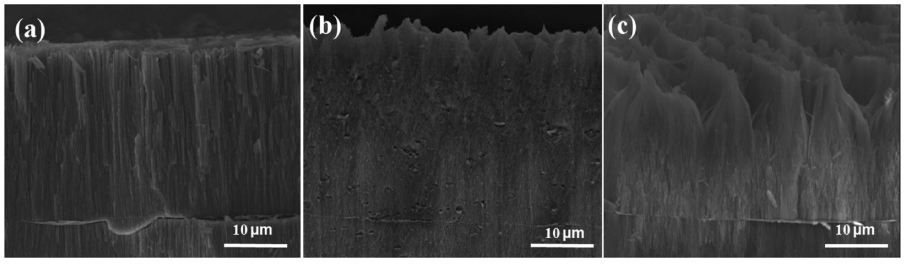

Figure 2. Corresponding side-view FESEM images of the anodized alumina membranes shown in Figure 1a–c.

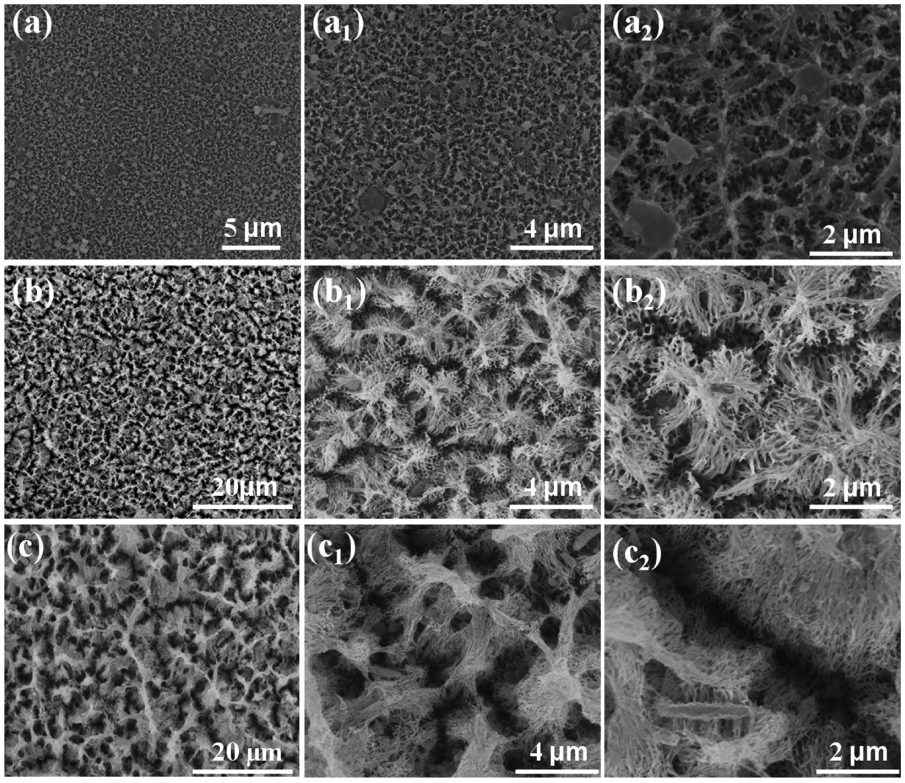

Figure 3. FESEM images of the Al plates anodized with diverse current densities under room temperature for 10 min. (a) 0.08 A/cm^2; (a_1) and (a_2) are the magnified images of (a). (b) 0.12 A/cm^2; (b_1) and (b_2) are the magnified images of (b). (c) 0.18 A/cm^2; (c_1) and (c_2) are the magnified images of (c).

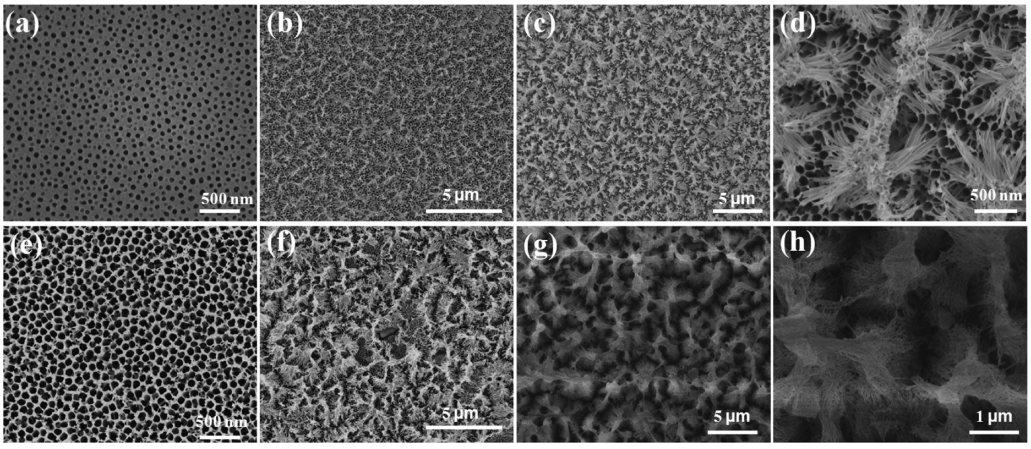

Figure 4. FESEM images of the Al plates anodized in diverse electrolyte temperatures at a current density of 0.16 A/cm^2. (a–c) Under the lower temperature of 0–10 °C and the anodization time of 3, 5, and 10 min, respectively. (d) High-magnification image of (c). (e–g) Under the higher temperature of 60–80 °C and the anodization time of 3, 5, and 10 min, respectively. (h) High-magnification image of (g).

acid under room temperature for 10 min. When the current density was controlled at 0.08 A/cm^2, only a small amount of nanowires formed on the surface (Figure 3a). From the high-magnification SEM images (Figure 3a_1 and a_2), it was found that most of the nanopores and nanowalls were broken and etched slightly and did not turn into nanowires. Anodizing for only 10 min was not long enough to produce large-area nanowires under the lower current density. As the current density increased to 0.12 A/cm^2, a very rough surface formed and large-area nanowires could be seen clearly (Figure 3b). The nanowires aggregated with each other and formed a kind of pyramid and ravine morphology (Figure 3b_1 and b_2). It also demonstrated that the current density of 0.12 A/cm^2 was sufficient to generate large-area nanowire pyramids within 10 min. With the increasing current density of 0.18 A/cm^2 (Figure 3c), we found that the surface became rougher and rougher. Meanwhile, the size of the nanowire pyramids and the ravines also obviously became larger and larger (Figure 3c_1 and c_2).

Figure 4 shows the fabrication results for diverse electrolyte temperatures (the electrolyte temperature here is controlled by a constant temperature magnetic stirrer). The other parameters are conducted in 0.3 M oxalic acid at 0.16 A/cm^2 current density for 10 min. As shown in Figure 4a–c, when the oxalic acid temperature is maintained at 5–10 °C, it confirms that the

dx.doi.org/10.1021/am4057858 | ACS Appl. Mater. Interfaces 2014, 6, 4831–4841

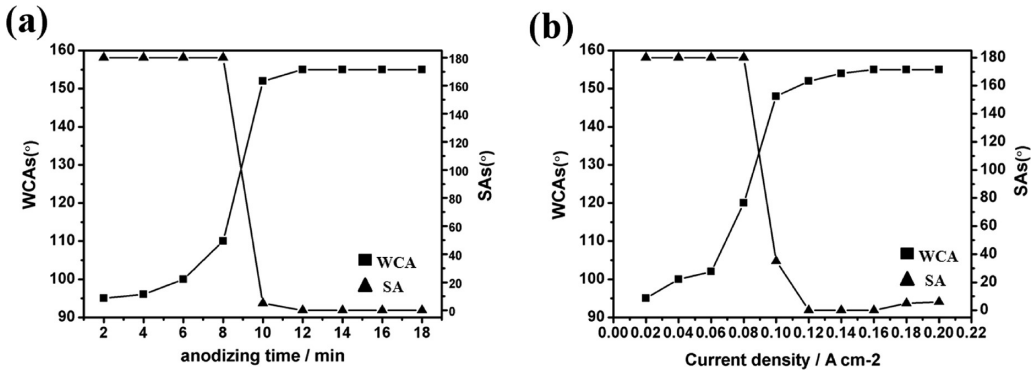

Figure 5. Corresponding WCAs and SAs of the anodized alumina membranes (the surfaces are all modified with PDES) fabricated under different reaction parameters. (a) Anodization time and (b) current density.

variation process of the morphology is similar to that in Figure 1 under room temperature. However, it can be seen that the nanopore structure tends to form more regularly (Figure 4a) under the lower temperature. The pore diameter anodized for 3 min is about 60 nm, which is smaller than that under room temperature (Figure 1a). When the anodization time is 5 min, it is found that a handful of nanowires are produced in this case, distributing sparsely on the surface, and the bottom nanopore structure can be observed from the top surface (Figure 4b). With the increasing anodization time of 10 min, a kind of order and regular pyramid and ravine structure can be seen on the top surface (Figure 4c). From the magnified SEM images (Figure 4d), we can observe that the diameters of each pyramid and ravine space are about 1 and 2 μm, respectively. The overall hierarchical structure is obviously more regular than the topography shown in Figure 1a. Actually, the lower reaction temperature can effectively decrease the extent of nanostructure destruction induced by heat, which also confirms that heat is one of the main reasons for formation of large-area nanowire structure. When the electrolyte temperature evaluated is more than 60 °C, the size of the nanopores becomes bigger up to 100 nm after anodization for 3 min, and it can also be observed that the top surface nanostructures are broken and etched more severely (Figure 4e). When anodized for 5 min, large-area nanowires densely cover the top surface (Figure 4f), and with increasing anodization time of 10 min, the denser and larger nanowire pyramid and ravine structure forms on the surface (Figure 4g and h). Unlike the morphology shown in Figure 4d, since the formation of the much higher aspect-ratio nanowire pyramids, the nanopore structure at the bottom cannot be seen from the top surface in Figure 4h.

We also investigate the effects of the anodization time, current density, and electrolyte temperature on surface wettability for water. Figure 5a presents the relationship of anodization time with the water contact angle and sliding angle. The other reaction conditions are controlled at 0.3 M oxalic acid under room temperature with the processing current density of 0.16 A/cm^2. The anodizing time ranges from 2 to 18 min. As the time increased, the WCA values show an increasing trend and the SA values have a large decreasing extent (in this work, we define the SA of the surface which has a WCA less than 150° but cannot repel the water droplets as 180°). Since the surface compositions of these surfaces are the same, we ascribe the wettability differences to the diverse surface roughness. With the production of the nanowire structure, the surface becomes rougher and rougher (see the surface morphology in Figure 1), finally resulting in a super-hydrophobic effect. Once the dual structures form on the surface, the surface can obtain superhydrophobicity with the WCA and SA of 155° and 0°, respectively, in 10 min. With the increasing reaction time of more than 10 min, the WCAs and the SAs almost have no change, indicating that the longer anodization time would not increase superhydrophobicity.

Figure 5b shows the relationship of the current density with the WCAs and SAs. The surface was electrochemically anodized in 0.3 M oxalic acid at room temperature for 10 min. The current density ranged from 0.02 to 0.2 A/cm^2. Due to the inability to obtain surface roughness sufficiently in 10 min under the lower current density of less than 0.12 A/cm^2, the as-prepared surface cannot achieve superhydrophobicity. It is found that when the current density was maintained higher than 0.12 A/cm^2, a superhydrophobic surface could be obtained and the rolling angle could also reach as low as 0°. With the increasing current density, the WCAs show an increasing trend. As we proposed previously, the current density determines the morphology of the surface. Under the higher current density of more than 0.12 A/cm^2, the hierarchical alumina pyramids-on-pores structure could form in 10 min and the sizes of the ravines and pyramids become larger with increasing current density (see the surface morphology in Figure 3), which would induce more air-pocket entrapment into the space, thus making the surface achieve better superhydrophobicity and sliding properties. However, we can notice that the SA values have a little increase when the current density is larger than 0.16 A/cm^2, indicating the decreasing sliding performance of the surface. In fact, although the size of the pyramids and ravines becomes larger under higher current density, we still consider that the bigger ravine structure would increase the adhesion between the surface and the water drop to some extent by the capillary forces, thus resulting in a little increase of SAs.

The effects of the electrolyte temperature on surface wettability were shown in Table 1. The aluminum plates were anodized in 0.3 M oxalic acid at a 0.16 A/cm^2 current density for 10 min. At the lower temperature region of 5−10 °C, we could learn that the surface was unable to achieve superhydrophobicity owing to the unavailable and insufficiently

Table 1. Effects of Temperature on Surface Wettability

temperature/°C	0−10	20−40	50−70	80−100
WCA/°	95	155	153	153
SA/°	180	0	6	10
the best time/min	20	10	8	5

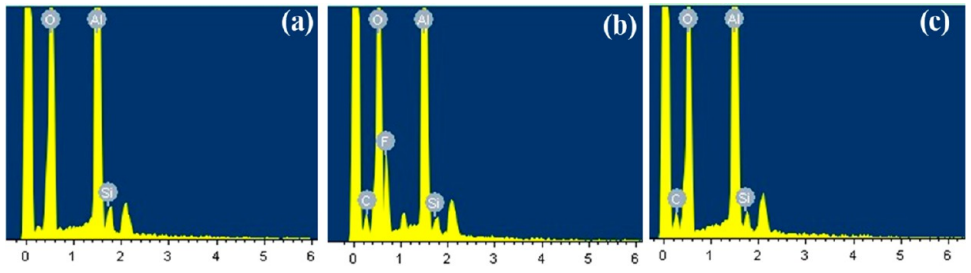

Figure 6. EDS spectra of the (a) unmodified HAPOP surface, (b) PDES-MS surface, (c) STA-MS surface.

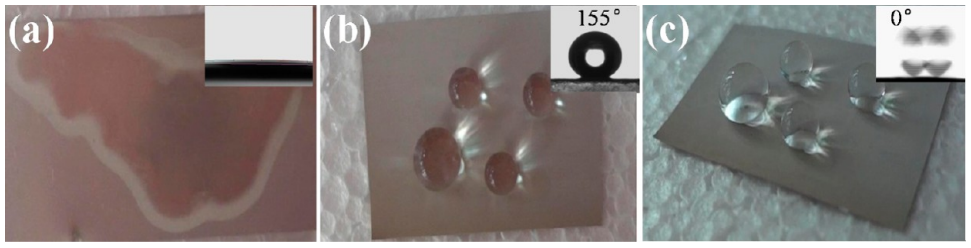

Figure 7. (a) Unmodified HAPOP surface shows superhydrophilicity with a WCA of 3°. (b) Top photograph of the water droplets on the PDES-MS surface. The inset indicates that the surface could obtain a WCA of 155°. (c) Side-view photograph of the water droplets. The inset shows that the surface presents a sliding behavior with an extremely low SA of 0°.

rough hierarchical structure with the inadequate anodized time. At the scope near room temperature, the surface can easily obtain slippery superhydrophobicity. However, when the temperature was higher than 60 °C, we found that anodization for 10 min would lead to a slight decrease of the superhydrophobic and slippery performance. The denser and larger-area nanowire architecture formed under the higher temperature would induce a decreasing amount and size of the ravine structures, which was not beneficial for air-pocket entrapment, hence resulting in reducing superhydrophobicity. We also summarize the most appropriate anodization time for achieving superhydrophobicity under each temperature scope (Table 1). This indicates that in order to construct the best superhydrophobic morphology, longer anodization time of 20 min is required under the lower temperature, while shorter time of 6 min is required under the higher temperature.

3.2. Analysis of the Resultant HAPOP Films Modified with Diverse Low Surface Energy Materials. *3.2.1. Chemical Compositions of the Diverse Samples.* In this paper, we use two kinds of materials (PDES, STA) to modify the HAPOP surface (the adopted HAPOP sample here was prepared at 0.3 M oxalic acid under room temperature with the current density of 0.16 A/cm^2 for 10 min). Figure 6a–c shows the EDS spectra of the untreated HAPOP, PDES-MS, and STA-MS surfaces. Compared with the unmodified HAPOP surface (Figure 6a), the extra elements C and F in Figure 6b, C in Figure 6c can be seen clearly, which highly corresponds to the chemical compositions of the two modifiers. XPS survey is also used to confirm that a layer of PDES or STA has been successfully self-assembled onto the surface (Figure S1). The compositions of these samples are calculated in detail and the results are summarized in Table S1.

3.2.2. Performance of the PDES-MS Surface. The chemical stability and mechanical durability of the PDES-MS and STA-MS surfaces are mainly evaluated and compared in this work. It is very delightful to find that the PDES-MS surface exhibits a series of excellent properties. Figure 7 shows the water droplets on the HAPOP surface before and after PDES modification. The HAPOP surface presents superhydrophilicity before modification (Figure 7a). The top-view and side-view pictures of the water droplets on the PDES-MS surface present perfect round shape (Figure 7b,c), indicating the achievement of superhydrophobicity after modification with PDES. It can achieve a WCA of 155° and a SA as low as 0° (the insets of Figure 7b and c). It is very obvious that the water droplets cannot stay at the surface due to its wonderful water-repellent ability (Video 1) and the large-scale superhydrophobic surface can be obtained through this method (Figure S2). The bouncing behavior is another outstanding performance of the PDES-MS surface. The surface cannot be wetted even when the droplet is hugely distorted (Figure S3). When the water droplets approach the surface from a certain height, they bounce very highly immediately and rebounce several times before they come to rest (Video 2). Actually, these nonwetting and bouncing properties of the superhydrophobic surface are very useful for waterproof fabrics that need to remain dry when exposed to raindrops and spraying tests.

The self-cleaning effect of the PDES-MS surface is shown in Figure 8. It can be seen clearly that the dusted carbon particles are washed away quickly by the continuing water drops. The surface becomes very clean in a short time, indicating an excellent antifouling ability of the surface. This means that the PDES-MS surface can protect the aluminum substrates from pollution in practical applications.

Due to the versatile and complex conditions in real life, the ability of superhydrophobic surfaces to withstand the harsh environments outside is a very significant consideration in practical applications. However, in the majority of the previous reports related to superhydrophobic surfaces, people usually use cool water (about 25 °C) to evaluate the wettability and adhesion performance of these superhydrophobic surfaces. There are few reports involving the repellent ability of the superhydrophobic surfaces to hot liquids.[17,41] Thus, from the view of practical applications, it is of great importance to examine the relationship between superhydrophobicity and hot liquids. In this paper, we use several kinds of hot liquids to

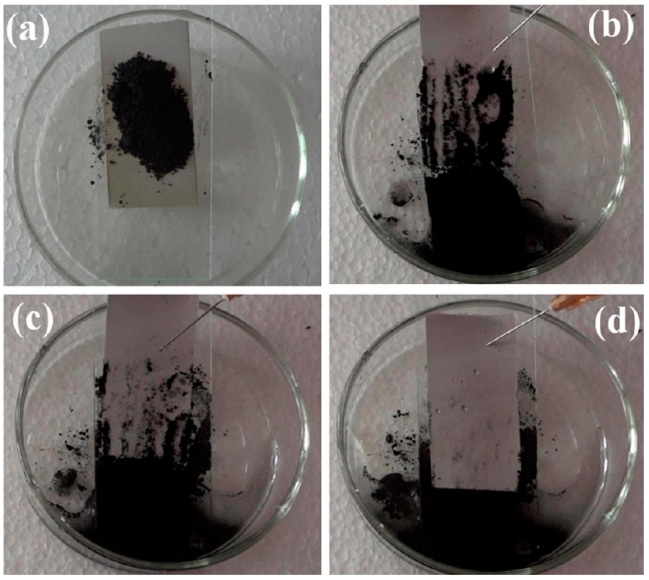

Figure 8. The self-cleaning process of the dusted carbon particles on the PDES-MS surface. (a) The surface was contaminated by mass carbon particles. (b–d) The surface became cleaner and cleaner with the continuing water droplets, and finally the particles were cleared up totally.

evaluate this ability of the PDES-MS surface. Figure 9a–f is the representative photographs of hot water, hot HCl (pH = 1) solution, hot NaOH (pH = 14) solution, hot milk, hot coffee, and hot tea droplets (the temperatures here of the liquids are around 80 °C) on the surface. All these liquid droplets maintain their round shape on the superhydrophobic surface. It can be observed that the surface can repel these diverse hot liquid droplets quickly without any trace (Video 3), presenting a wonderful liquid-repellent property. These phenomena sufficiently indicate that the as-prepared PDES-MS surface has an excellent ability to resist hot liquids, which is scarcely realized in most superhydrophobic surfaces. We then systematically study the repellent behaviors of the PDES-MS surface to diverse liquids (water, HCl/NaOH solutions) at different temperatures. As indicated in Figure 9g, the superhydrophobic surface can repel cool liquids (around 30 °C) very quickly and the sliding properties of the cool HCl/NaOH solution droplets are the same as those of cool water, which could also achieve WCA of 155° and SA of 0°. As the temperature of the liquids increased, the WCAs and SAs of the surface to water droplets are almost unchanged and the superhydrophobicity can also be maintained toward hot HCl/NaOH solution droplets (even at 100 °C). However, the SA values become larger with increasing temperature, which demonstrates that the surface becomes a little sticky toward the liquids at higher temperature. Even so, the relatively small changes about the WCA and SA values further confirm that our as-prepared PDES-MS surface is highly stable against chemical corrosion and high liquid temperature. We also investigate the stability of the PDES-MS surface under many other harsh conditions. As shown in Figure 9h, the WCAs are maintaind above 150° and the SAs remain below 10° after the PDES-MS surface is soaked in various organic solvents

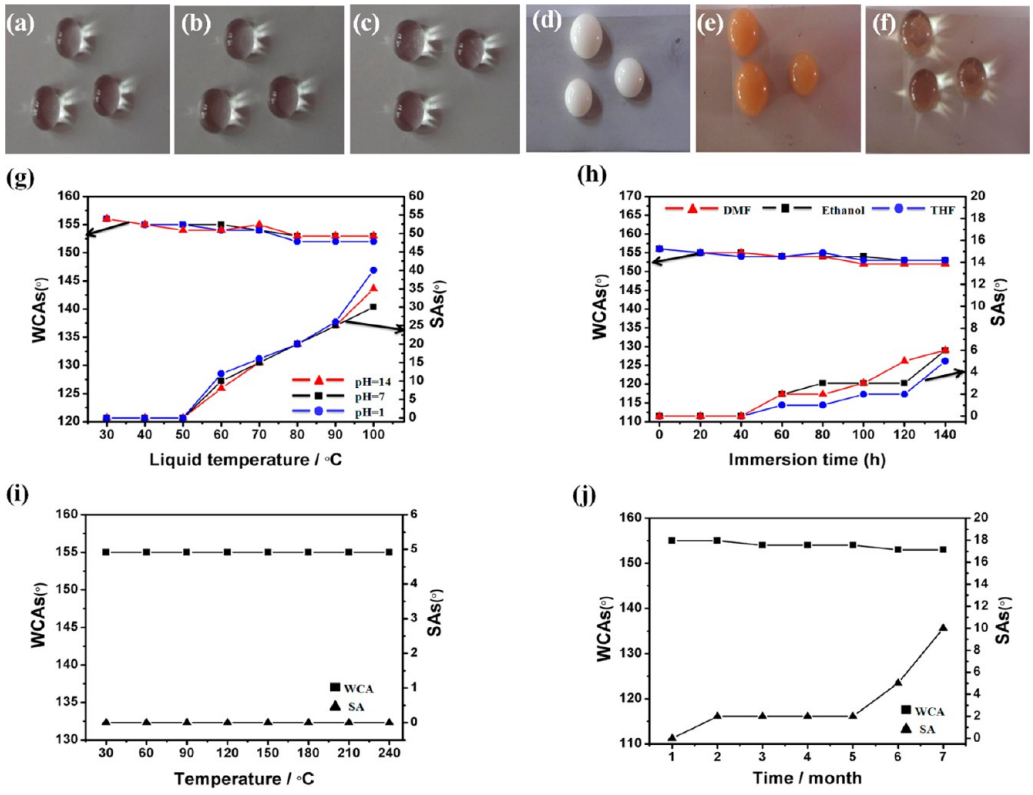

Figure 9. Photographs of the diverse liquid droplets on the PDES-MS surface. (a–f) The liquid droplets are hot water, hot HCl solution, hot NaOH solution, hot milk, hot coffee, and hot tea sequentially (the temperature of these liquids are around 80 °C). The variations of water repellency of the PDES-MS surface under various harsh conditions: (g) when it was wetted by HCl (pH = 1), water (pH = 7), NaOH (pH = 14) under the various higher liquid temperature scope of 30–100 °C, (h) immersion in diverse organic solvents, (i) after it was placed under room temperature condition for diverse periods of time, (j) different surface temperatures of 30–250 °C.

dx.doi.org/10.1021/am4057858 | ACS Appl. Mater. Interfaces 2014, 6, 4831–4841

including dimethyl formamide (DMF), ethanol, and THF for 24 h. When the PDES-MS surface is exposed to high temperature conditions, it seems that the surface temperature does not induce any change of the WCAs and SAs. As indicated in Figure 9i, the WCAs and SAs of the surface always remain at 155° and 0° even when the surface temperature is as high as 250 °C, which further demonstrates the excellent superhydrophobic stability of the PDES-MS surface. The surface still presents fascinating stability during a long time period. After 7 months, the WCA and SA can still achieve 151° and 8°, respectively (Figure 9j).

Although large numbers of artificial superhydrophobic surfaces have been achieved, many surfaces suffer mechanical damage or susceptibility to mechanical press. Moreover, most superhydrophobic surfaces with high roughness tend to be delicate and thus easily lose the superhydrophobicity when touched. For example, when a synthetic superhydrophobic surface is touched by a bare hand, the affected area of the surface would be contaminated by salt and oil, which would increase surface energy and finally result in losing superhydrophobicity. In short, up to now, the mechanical durability of the superhydrophobic surface is still a seriously urgent problem. However, we find that the PDES-MS surface prepared in our work could effectively resist the above problems. Our qualitative experimental results on the mechanical properties of the as-prepared PDES-MS surface are shown in Figure S4; it can be observed that the PDES-MS surface can still maintain superhydrophobicity even after multiple folding or finger-contact treatment, indicating its outstanding mechanical durability. Unlike the uneven and unstable superhydrophobic layer fabricated by some normally used methods (such as solution-immersion, plasma etching, chemical vapor deposition methods), the PDES-MS surface obtained through the anodization technique could successfully avoid this problem. Figure 10 displays the PDES-MS surface before (Figure 10a)

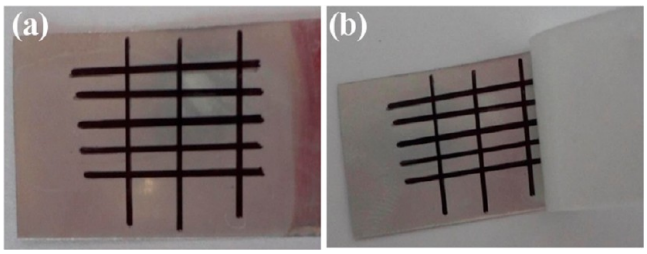

Figure 10. Photograph of the PDES-MS surface (a) before and (b) after the cross cut tape test.

and after (Figure 10b) the cross cut tape test. The pattern on the surface is not removed after the removal of the tape, which confirms that the superhydrophobic membrane layer adheres to the aluminum substrate firmly. The WCAs of the surface before and after the cross cut tape test are almost the same. The excellent attachment between the superhydrophobic layer and the substrate of the PDES-MS surface can also be confirmed by the ultrsonication test. Figure 11a is the variation of WCAs and SAs after ultrasonication of the PDES-MS surface in ethanol for diverse times. It is found that the WCAs and SAs vary only slightly even after they have been ultrasonicated for 14 h, further indicating that the adhesion between the superhydrophobic alumina film and the aluminum substrate is very secure. The mechanical performance of the PDES-MS surface was further evaluated by abrading the sample back and forth onto sandpaper at a rate of 5 cm s^{-1} under 200 g of force for various repeated cycles (Figure S5). The results were concluded in Figure 11b. Although the SA obviously increased to 40° after the sample was rubbed 50 times, the WCA still remained above 150°, which indicated that the surface had excellent mechanical damage resistance. Figure 11c–shows the SEM images of the PDES-MS surface that had been rubbed for 10, 30, and 50 cycles. The results demonstrated that although some of the top nanobumps were damaged, the nanoscaled tanglesome nanowires of the surface were still retained (the inset in Figure 11e,f), which were responsible for the maintained superhydrophobicity of the PDES-MS surface even when it was rubbed for 50 cycles. The abrasion resistance of the superhydrophobic surface could also be confirmed by Video 4, when the surface was abraded by the sandpaper, water droplets still slide easily from the surface. It was also found that the surface could regain its lost superhydrophobicity quickly after it was modified with PDES monolayer again (Figure S6). Furthermore, as shown by the XPS and EDS composition analysis of the surface after abrasion (Figure S7 and Table S2), we found that the amount of fluorine after 5, 10, and 20 cycles of abrasion test decreased slightly compared to that before the abrasion test. These results indicate that the PDES molecules have a relatively strong combination with the HAPOP surface and the consumption of the PDES molecules in each abrasion treatment is only a small part of the total molecule concentration preserved in the surface. The small loss of the low surface energy hydrophobic layer contents, when combined with the maintained rough textures, gives rise to the durable superhydrophobicity of the PDES-MS surface.

All of the above results demonstrate that our as-prepared PDES-MS surface is highly stable and robust, which could find significantly practical applications in industrial areas under rigorous conditions.

3.2.3. Performances of the STA-MS Surface. Compared with fluorocarbon-terminated modifier, stearic acid (STA, alkyl-terminated molecular) is much cheaper and is also used to coat the rough structure to achieve superhydrophobicity. The shapes of water CA, water SA, and hexadecane CA on STA-MS surface are displayed in Figure 12. It shows that the STA-MS surface can achieve superhydrophobicity with the WCA and SA of 153° and 0° (Figure 12a and b), respectively. The hexadecane CA on PDES-MS surface can reach 85°; however, when the hexadecane droplet approaches the STA-MS surface, it spreads and infiltrates into the surface quickly, presenting a superoleophilic property with a hexadecane CA of 0° (Figure 12c). The STA-MS surface is also proven to possess extremely slippery and nonwetting performance; the water droplets also bounce immediately when they approach STA-MS surfaces. These results demonstrate that the finely constructed hierarchical nanowire pyramids-on-pores structure is the more prevailing factor than surface energy in making the superhydrophobic surface achieve excellent nonwetting and slippery performance. Moreover, as shown in Figure 13, when the STA-MS surface was wetted by mass hexadecane, the water droplets can still slide easily. Next, we then evaluate the stability of the STA-MS surface by using the same methods as with the PDES-MS surface. The results are displayed in Table S3. It is found that the STA-MS surface cannot resist hot water droplets with the temperature higher than 40 °C, to say nothing of the hot acid/alkali solution. Previous study has proposed that the ability of the surface to repel hot liquids is more related with surface energy than surface roughness.[17] Since the STA has a higher

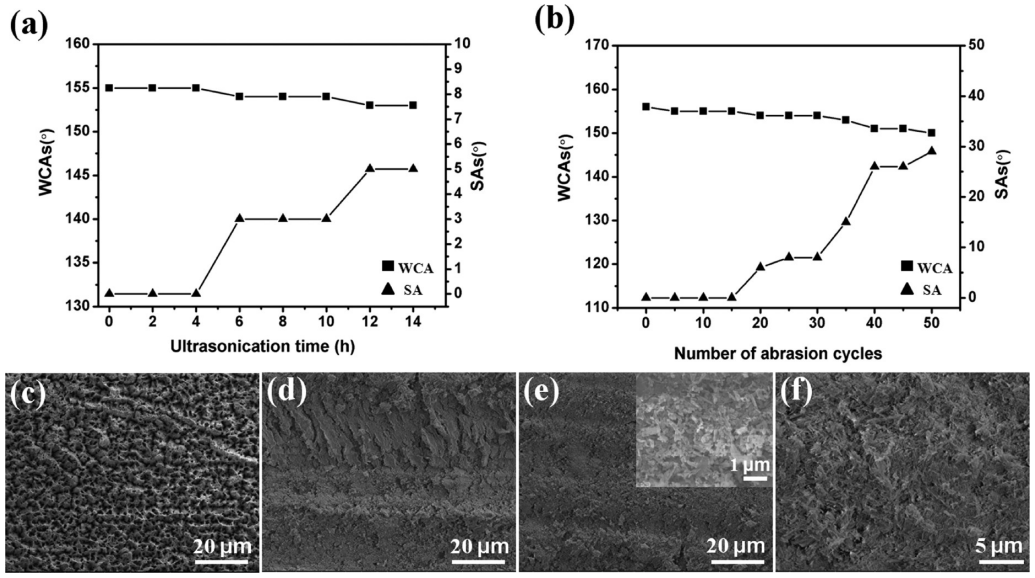

Figure 11. The mechanical stability of the PDES-MS surface was evaluated by various tests, such as (a) ultrasonication treatment in ethanol solvent and (b) abrasion of the PDES-MS surface with sandpaper. SEM images of the original PDES-MS surface (c) and after it had been rubbed for 10 (d), 30 (e), and 50 (f) cycles with sandpaper.

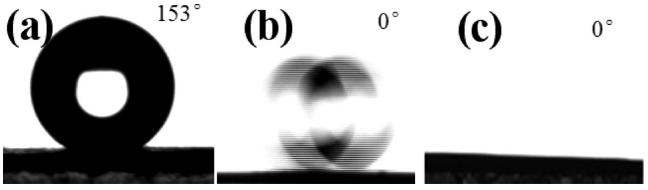

Figure 12. The shape, the sliding behavior of water droplets, and the shape of the hexadecane droplet on the STA-MS surface, presenting a WCA and a SA of 153° (a) and 0° (b), respectively, and achieving superoleophilicity with a hexadecane CA of 0° (c).

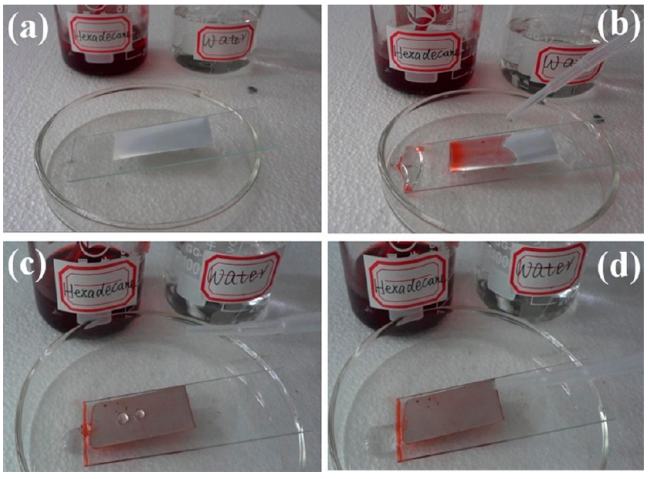

Figure 13. The rolling process of the water droplets on the hexadecane oil-wetting STA-MS surface. (a,b) The surface was superoleophilic and the hexadecane droplets immersed into the surface. (c,d) the water droplets can still slide from the hexadecane oil-contaminated surface.

surface free energy than PDES, the ability of the STA-MS surface to resist hot liquids is much worse than that of the PDES-MS surface. When we study the mechanical durability of the STA-MS surfaces, it is found that the STA-MS surface could only support 10 abrasion cycles at maximum (Table S3), which is far less than the PDES-MS surface. This may be due to the bonding between the STA layer and the alumina substrate being much weaker than PDES-MS surface, resulting in greater STA loss after each abrasion test. These results further demonstrate that the surface energy of the modifier and the bonding between the modifier molecules and the substrate significantly affect the chemical stability and mechanical durability of the superhydrophobic surfaces. Compared with the STA-MS surface, the superior chemical stability and mechanical durability shown by the PDES-MS surface are attributed to its lower surface energy and its relatively strong molecular bonding with the alumina substrate.

3.2.4. Corrosion Resistance of the PDES (STA)-MS Surfaces. In order to investigate the effects of the superhydrophobic films on the corrosion resistance of the aluminum substrate, the potentiodynamic polarization curves of the unmodified and PDES (STA)-MS surfaces in the 3.5 wt % NaCl aqueous solution are obtained using the Tafel extrapolation method and are presented in Figure 14. A close inspection of the data reveals that the corrosion potentials

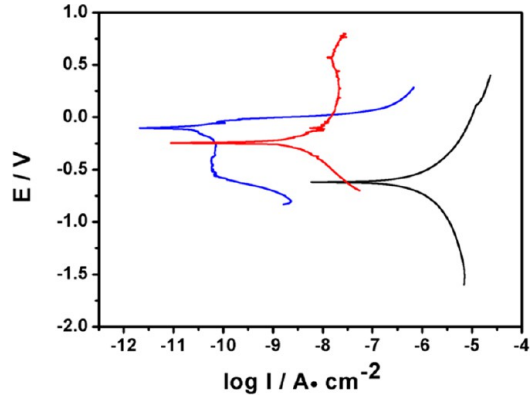

Figure 14. Potentiodynamic polarization curves of the unmodified HAPOP surface and PDES (STA)-MS surfaces in 3.5 wt % NaCl aqueous solution.

dx.doi.org/10.1021/am4057858 | ACS Appl. Mater. Interfaces 2014, 6, 4831−4841

(E_{corr}) of both the PDES-MS and STA-MS surfaces are more positive than that of the unmodified HAPOP surface, suggesting good protection for aluminum substrate through the superhydrophobic films. The corrosion current density (I_{corr}) of the unmodified surface is 9.70×10^{-8} A/cm^2, whereas those of STA-MS and PDES-MS surfaces are 5.13×10^{-10} and 1.31×10^{-11} A/cm^2, respectively. It is worth noting that the corrosion densities are reduced by more than 2 orders for STA-MS surface and 3 orders for PDES-MS surface in comparison with the unmodified surface. Such low current density demonstrates an excellent corrosion resistance of the two superhydrophobic surfaces. However, when viewed from the data, the value of the E_{corr} of the PDES-MS surface is more positive than the STA-MS surface, while that of the I_{corr} value is smaller, which indicates that the corrosion resistance of PDES-MS surface is more superb than that of the STA-MS surface. In fact, we find that the WCA and SA values of the tested area of the PDES-MS surface have almost no change, further indicating its marvelous stability.

3.2.5. Surface Free Energy of the Different Surfaces. The above results demonstrate that the chemical stability and mechanical durability of the PDES-MS surface are much more superior than that of the STA-MS surface. We then measure the surface free energy of the PDES-MS and STA-MS surfaces and summarize them in Table 2. When compared with the flat aluminum surface, the surface free energy values of the two kinds of samples decrease greatly after the modification treatment. The STA-MS has the value of 16.08 mJ/m^2, while that of the PDES-MS surface can reach as low as 0.78 mJ/m^2, which is far smaller than 16.08 mJ/m^2. These results can be used to further demonstrate and account for the huge performance differences between the PDES-MS and STA-MS surfaces.

Table 2. Summary of Surface Free Energy of the Diverse-Modified Surfaces

sample	θ_e^{water} (deg)	$\theta_e^{diiodomethane}$ (deg)	γ^{polar} (mJ/m^2)	$\gamma^{dispersive}$ (mJ/m^2)	γ (mJ/m^2)
flat aluminum	82.7	38	1.17	39.44	40.61
PDES-MS	155.5	140.5	0.04	0.74	0.78
STA-MS	155.1	100	4.91	11.17	16.08

4. CONCLUSIONS

We have introduced a highly effective and easy-to-implement method to fabricate chemically stable and mechanically robust superhydrophobic alumina surface on Al substrate. The effects of the processing parameters including the anodization time, the current density, and the electrolyte temperature on surface morphology and surface wettability have been investigated in detail. These parameters hugely affect the surface architectures that influence the surface hydrophobicity significantly. It is demonstrated that the hierarchical alumina pyramids-on-nanopores (HAPOP) morphology is necessary to attain superhydrophobicity. The rough HAPOP surface which can be obtained quickly at 0.3 M oxalic aicd under room temperature with a current density of 0.16 A/cm^2 within 10 min, together with two kinds of modifier (PDES, STA) deposition could result in the achievement of excellent nonwetting and extremely slippery behaviors.

The chemical stability and mechanical durability of the PDES-MS and STA-MS surfaces are evaluated and investigated. Compared with the STA-MS surface, the resulting PDES-MS surface achieves a WCA of 155° and a SA as low as 0°. What is most important is that it exhibits amazing and fascinating superhydrophobic stability and mechanical durability. It has an excellent resistance toward a series of harsh conditions such as hot liquids including hot water (30−100 °C), hot corrosive liquids (HCl/NaOH solutions, 30−100 °C), hot beverages (coffee, milk, tea, 80 °C), various solvent immersion, high temperature, and long time period. It also shows outstanding mechanical properties which could resist ultrasonication treatment, finger-touch, multiple fold, peeling by adhesive tape, and even abrasion test treatments for 50 cycles under 200 g of force. The STA-MS surface obtains a WCA of 153° and SA of 0°. It shows superoleophobicity with a hexadecane CA of 0°. However, the STA-MS surface is demonstrated to show much worse resistance to hot liquids or abrasion treatment than PDES-MS surface. The corrosion resistance of the PDES (STA)-MS surfaces was measured in 3.5 wt % NaCl solution. The results proved that the superhydrophobic deposition layer could effectively protect the aluminum substrate from corrosive solution in comparison with the bare aluminum foil. However, the PDES-MS surface still exhibits more excellent corrosion resistance than the STA-MS surface. The superior chemical stability and mechanical durability shown by the PDES-MS surface are believed to attribute to its lower surface energy and its relatively stronger molecular bonding with the alumina substrate. Our fabrication process is simple, highly efficient, and cost-effective. Hence, the present method must be very suitable and highly effective for preparing a large-area superhydrophobic alumina surface with high chemical stability and excellent mechanical durability.

■ ASSOCIATED CONTENT

Ⓢ Supporting Information

Additional figures and data tables. Video S1: excellent large-scale superhydrophobic performance. Video S2: fascinating bouncing behavior. Video S3: hot liquid-repellent process. Video S4: abrasion process of the resultant superhydrophobic surface. This material is available free of charge via the Internet at http://pubs.acs.org.

■ AUTHOR INFORMATION

Corresponding Author

*Phone: (+86)020-22236708. E-mail: wldeng@scut.edu.cn.

Notes

The authors declare no competing financial interest.

■ ACKNOWLEDGMENTS

Financial support from the National Natural Science Foundation of China (51373055 and 21103053), the National Program on Key Basic Research Project (2012CB932900), and the Cooperation Project in Industry, Education and Research of Guangdong Province and Ministry of Education of China (No. 2011B090400376) are gratefully acknowledged.

■ REFERENCES

(1) Gao, X.; Jiang, L. Biophysics: Water-Repellent Legs of Water Striders. *Nature* **2004**, *432*, 36−36.

(2) Barthlott, W.; Neinhuis, C. Purity of the Sacred Lotus, Or Escape from Contamination in Biological Surfaces. *Planta* **1997**, *202*, 1−8.

(3) Lai, Y. K.; Chen, Z.; Lin, C. J. Recent Progress on the Superhydrophobic Surfaces with Special Adhesion: From Natural to Biomimetic to Functional. *J. Nanoeng. Nanomanuf.* **2011**, *1*, 18−34.
(4) Abbott, N. L.; Folkers, J. P.; Whitesides, G. M. Manipulation of the Wettability of Surfaces on the 0.1- to 1-Micrometer Scale Through Micromachining and Molecular Self-Assembly. *Science* **1992**, *257*, 1380−1382.
(5) Gau, H.; Herminghaus, S.; Lenz, P.; Lipowsky, R. Liquid Morphologies on Structured Surfaces: From Microchannels to Microchips. *Science* **1999**, *283*, 46−49.
(6) Li, Y.; Liu, F.; Sun, J. A Facile Layer-by-Layer Deposition Process for the Fabrication of Highly Transparent Superhydrophobic Coatings. *Chem. Commun.* **2009**, 2730−2732.
(7) Zheng, L.; Li, Z.; Bourdo, S.; Saini, V.; Ryerson, C.; Biris, A. S. Hierarchical ZnO Structure with Superhydrophobicity and High Adhesion. *ChemPhysChem* **2011**, *12*, 2412−2414.
(8) Saleema, N.; Sarkar, D.; Gallant, D.; Paynter, R.; Chen, X.-G. Chemical Nature of Superhydrophobic Aluminum Alloy Surfaces Produced via a One-Step Process Using Fluoroalkyl-Silane in a Base Medium. *ACS Appl. Mater. Interfaces* **2011**, *3*, 4775−4781.
(9) Qian, B.; Shen, Z. Fabrication of Superhydrophobic Surfaces by Dislocation-Selective Chemical Etching on Aluminum, Copper, And Zinc Substrates. *Langmuir* **2005**, *21*, 9007−9009.
(10) Ganesh, V. A.; Nair, A. S.; Raut, H. K.; Tan, T. T. Y.; He, C.; Ramakrishna, S.; Xu, J. Superhydrophobic Fluorinated POSS-PVDF-HFP Nanocomposite Coating on Glass by Electrospinning. *J. Mater. Chem.* **2012**, *22*, 18479−18485.
(11) Lin, J.; Cai, Y.; Wang, X.; Ding, B.; Yu, J.; Wang, M. Fabrication of Biomimetic Superhydrophobic Surfaces Inspired by Lotus Leaf and Silver Ragwort Leaf. *Nanoscale* **2011**, *3*, 1258−1262.
(12) Li, X.; Shen, J. A Facile Two-Step Dipping Process Based on Two Silica Systems for a Superhydrophobic Surface. *Chem. Commun.* **2011**, *47*, 10761−10763.
(13) Lee, M.; Kwak, G.; Yong, K. Wettability Control of ZnO Nanoparticles for Universal Applications. *ACS Appl. Mater. Interfaces* **2011**, *3*, 3350−3356.
(14) Wu, W.; Wang, X.; Wang, D.; Chen, M.; Zhou, F.; Liu, W.; Xue, Q. Alumina Nanowire Forests via Unconventional Anodization and Super-Repellency Plus Low Adhesion to Diverse Liquids. *Chem. Commun.* **2009**, 1043−1045.
(15) Xu, W.; Song, J.; Sun, J.; Lu, Y.; Yu, Z. Rapid Fabrication of Large-Area, Corrosion-Resistant Superhydrophobic Mg Alloy Surfaces. *ACS Appl. Mater. Interfaces* **2011**, *3*, 4404−4414.
(16) Kim, Y.; Lee, S.; Cho, H.; Park, B.; Kim, D.; Hwang, W. Robust Superhydrophilic/Hydrophobic Surface Based on Self-Aggregated Al_2O_3 Nanowires by Single-Step Anodization and Self-Assembly Method. *ACS Appl. Mater. Interfaces* **2012**, *4*, 5074−5078.
(17) Liu, Y.; Chen, X.; Xin, J. Can Superhydrophobic Surfaces Repel Hot Water? *J. Mater. Chem.* **2009**, *19*, 5602−5611.
(18) Yang, J.; Zhang, Z.; Men, X.; Xu, X.; Zhu, X. A Simple Approach to Fabricate Superoleophobic Coatings. *New J. Chem.* **2011**, *35*, 576−580.
(19) Zhu, X.; Zhang, Z.; Xu, X.; Men, X.; Yang, J.; Zhou, X.; Xue, Q. Facile Fabrication of a Superamphiphobic Surface on the Copper Substrate. *J. Colloid Interface Sci.* **2012**, *367*, 443−449.
(20) Kannarpady, G. K.; Khedir, K. R.; Ishihara, H.; Woo, J.; Oshin, O. D.; Trigwell, S.; Ryerson, C.; Biris, A. S. Controlled Growth of Self-Organized Hexagonal Arrays of Metallic Nanorods Using Template-Assisted Glancing Angle Deposition for Superhydrophobic Applications. *ACS Appl. Mater. Interfaces* **2011**, *3*, 2332−2340.
(21) Bae, W. G.; Song, K. Y.; Rahmawan, Y.; Chu, C. N.; Kim, D.; Chung, D. K.; Suh, K. Y. One-Step Process for Superhydrophobic Metallic Surfaces by Wire Electrical Discharge Machining. *ACS Appl. Mater. Interfaces* **2012**, *4*, 3685−3691.
(22) Höhne, S.; Blank, C.; Mensch, A.; Thieme, M.; Frenzel, R.; Worch, H.; Müller, M.; Simon, F. Superhydrophobic Alumina Surfaces Based on Polymer-Stabilized Oxide Layers. *Macromol. Chem. Phys.* **2009**, *210*, 1263−1271.
(23) Saleema, N.; Sarkar, D.; Paynter, R.; Chen, X.-G. Superhydrophobic Aluminum Alloy Surfaces by a Novel One-Step Process. *ACS Appl. Mater. Interfaces* **2010**, *2*, 2500−2502.
(24) Guo, Z.; Zhou, F.; Hao, J.; Liu, W. Stable Biomimetic Super-Hydrophobic Engineering Materials. *J. Am. Chem. Soc.* **2005**, *127*, 15670−15671.
(25) Lu, S.; Chen, Y.; Xu, W.; Liu, W. Controlled Growth of Superhydrophobic Films by Sol−Gel Method on Aluminum Substrate. *Appl. Surf. Sci.* **2010**, *256*, 6072−6075.
(26) Xu, Q. F.; Wang, J. N. A Superhydrophobic Coating on Aluminium Foil with an Anti-Corrosive Property. *New J. Chem.* **2009**, *33*, 734−738.
(27) Liu, L.; Zhao, J.; Zhang, Y.; Zhao, F.; Zhang, Y. Fabrication of Superhydrophobic Surface by Hierarchical Growth of Lotus-Leaf-Like Boehmite on Aluminum Foil. *J. Colloid Interface Sci.* **2011**, *358*, 277−283.
(28) Yao, L.; Zheng, M.; Ma, L.; Li, W.; Li, M.; Shen, W. Self-Assembly of Diverse Alumina Architectures and Their Morphology-Dependent Wettability. *Mater. Res. Bull.* **2011**, *46*, 1403−1408.
(29) Jeong, C.; Choi, C.-H. Single-Step Direct Fabrication of Pillar-on-Pore Hybrid Nanostructures in Anodizing Aluminum for Superior Superhydrophobic Efficiency. *ACS Appl. Mater. Interfaces* **2012**, *4*, 842−848.
(30) Peng, S.; Tian, D.; Miao, X.; Yang, X.; Deng, W. Designing Robust Alumina Nanowires-on-Nanopores Structures: Superhydrophobic Surfaces with Slippery or Sticky Water Adhesion. *J. Colloid Interface Sci.* **2013**, *409*, 18−24.
(31) Barthwal, S.; Kim, Y. S.; Lim, S.-H. Mechanically Robust Superamphiphobic Aluminum Surface with Nanopore-Embedded Microtexture. *Langmuir* **2013**, *29*, 11966−11974.
(32) Zhu, Q.; Chu, Y.; Wang, Z.; Chen, N.; Lin, L.; Liu, F.; Pan, Q. Robust Superhydrophobic Polyurethane Sponge As a Highly Reusable Oil-Absorption Material. *J. Mater. Chem. A* **2013**, *1*, 5386−5393.
(33) Wang, H.; Xue, Y.; Ding, J.; Feng, L.; Wang, X.; Lin, T. Durable, Self-Healing Superhydrophobic and Superoleophobic Surfaces from Fluorinated-Decyl Polyhedral Oligomeric Silsesquioxane and Hydrolyzed Fluorinated Alkyl Silane. *Angew. Chem., Int. Ed.* **2011**, *50*, 11433−11436.
(34) Deng, B.; Cai, R.; Yu, Y.; Jiang, H.; Wang, C.; Li, J.; Li, L.; Yu, M.; Li, J.; Xie, L. Laundering Durability of Superhydrophobic Cotton Fabric. *Adv. Mater.* **2010**, *22*, 5473−5477.
(35) Zimmermann, J.; Reifler, F. A.; Fortunato, G.; Gerhardt, L. C.; Seeger, S. A Simple, One-Step Approach to Durable and Robust Superhydrophobic Textiles. *Adv. Funct. Mater.* **2008**, *18*, 3662−3669.
(36) Chen, X.; Yang, G.; Kong, L.; Dong, D.; Yu, L.; Chen, J.; Zhang, P. Different Wetting Behavior of Alkyl-and Fluorocarbon-Terminated Films Based on Cupric Hydroxide Nanorod Quasi-Arrays. *Mater. Chem. Phys.* **2010**, *123*, 309−313.
(37) Chen, X.; Kong, L.; Dong, D.; Yang, G.; Yu, L.; Chen, J.; Zhang, P. Fabrication of Functionalized Copper Compound Hierarchical Structure with Bionic Superhydrophobic Properties. *J. Phys. Chem. C* **2009**, *113*, 5396−5401.
(38) Han, J.; Kim, J.; Choi, Y.; Chang, K.-S.; Lee, J.; Youn, H.; Bu, S. Structure of Alumina Nanowires Synthesized by Chemical Etching of Anodic Alumina Membrane. *Phys. E* **2007**, *36*, 140−146.
(39) Xiao, Z.; Han, C. Y.; Welp, U.; Wang, H.; Kwok, W.; Willing, G.; Hiller, J.; Cook, R.; Miller, D.; Crabtree, G. Fabrication of Alumina Nanotubes and Nanowires by Etching Porous Alumina Membranes. *Nano Lett.* **2002**, *2*, 1293−1297.
(40) Li, Y.; Ling, Z.; Chen, S.; Hu, X.; He, X. Novel AAO Films and Hollow Nanostructures Fabricated by Ultra-High Voltage Hard Anodization. *Chem. Commun.* **2010**, *46*, 309−311.
(41) Wang, S.; Feng, L.; Jiang, L. One-Step Solution-Immersion Process for the Fabrication of Stable Bionic Superhydrophobic Surfaces. *Adv. Mater.* **2006**, *18*, 767−770.